Supporting Information for "Physics-informed neural networks for Richardson-Richards equation: Estimation of constitutive relationships and soil water flux density from volumetric water content measurements"

Toshiyuki Bandai [1], Teamrat A. Ghezzehei [1]

[1]Life and Environmental Science Department, University of California, Merced, 5200, Lake Rd, Merced, CA, 95343, USA

Contents of this file

1. Figures S1 to S9
2. Tables S1 to S6

Introduction In this material, figures and tables which could not be shown in the main manuscript are provided. Figure S1 shows an example of the minimization of the loss function through Adam (Kingma & Ba, 2014) and L-BFGS-B (Byrd et al., 1995) algorithms. Figure S2 and S3 shows soil moisture dynamics at three different depths for loam and silt loam soil respectively. The residual of the Richardson-Richards equation at three different depths for loam and silt loam soil are shown in the Figure S4 and S5 respectively. Figure S6 shows the estimated soil water flux density against the true value for all the three soils for the two scenarios. Figure S7, S8, and S9 help the reader to compare the estimated soil water flux density to the true value for a limited range.

The tables are the information about the architecture of the neural networks used in the physics-informed neural networks (PINNs). Table S1 shows the effect of noise added to the synthetic volumetric water content measurements. Table S2 and S3 summarizes the investigations on the number of hidden layers and units used in the neural networks for the predicted matric potential for sandy loam and loam soil. Table S4, S5, and S6 shows the effect of the number of units of the hidden layer of the neural networks for predicted volumetric water content and hydraulic conductivity.

References

Byrd, R. H., Lu, P., Nocedal, J., & Zhu, C. (1995). A limited memory algorithm for bound constrained optimization. *Journal of Scientific Computing*, *16*(5), 1190–1208. doi: 10.1137/0916069

Kingma, D. P., & Ba, J. B. (2014). Adam: A method for stochastic optimization. *arXiv preprint*, 1–15. Retrieved from `https://arxiv.org/pdf/1412.6980.pdf`

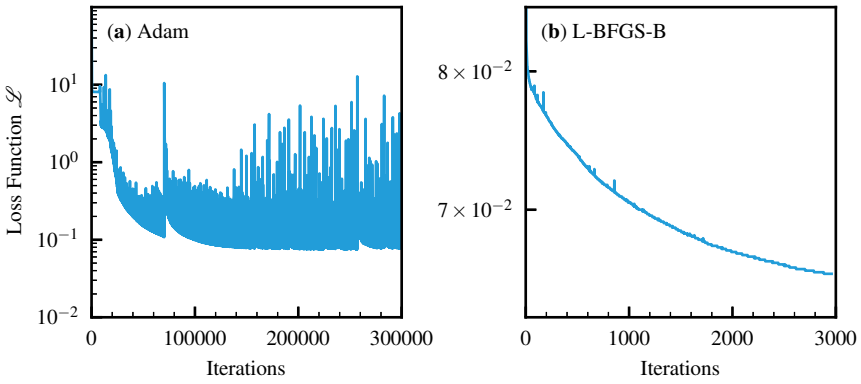

Figure S1. Minimization of loss function for sandy loam soil for Scenario 2. (**a**) Adam algorithm (Kingma & Ba, 2014). (**b**) L-BFGS-B algorithm (Byrd et al., 1995).

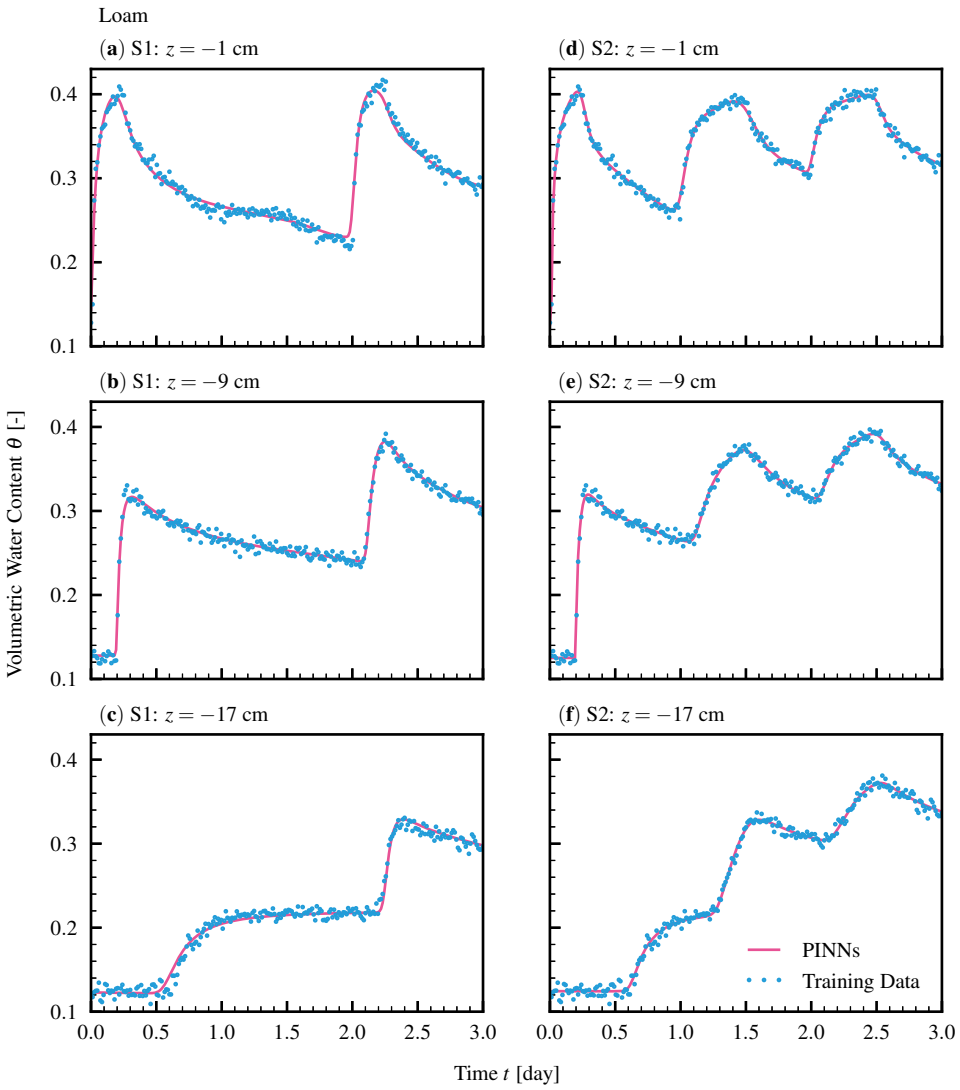

Figure S2. Predicted volumetric water content (PINNs) and noisy synthetic training data (Training Data) for loam soil for the two scenarios at three different depths. Scenario 1 (S1): (**a**) $z = -1$ cm, (**b**) $z = -9$ cm, and (**c**) $z = -17$ cm. Scenario 2 (S2): (**d**) $z = -1$ cm, (**e**) $z = -9$ cm, and (**f**) $z = -17$ cm.

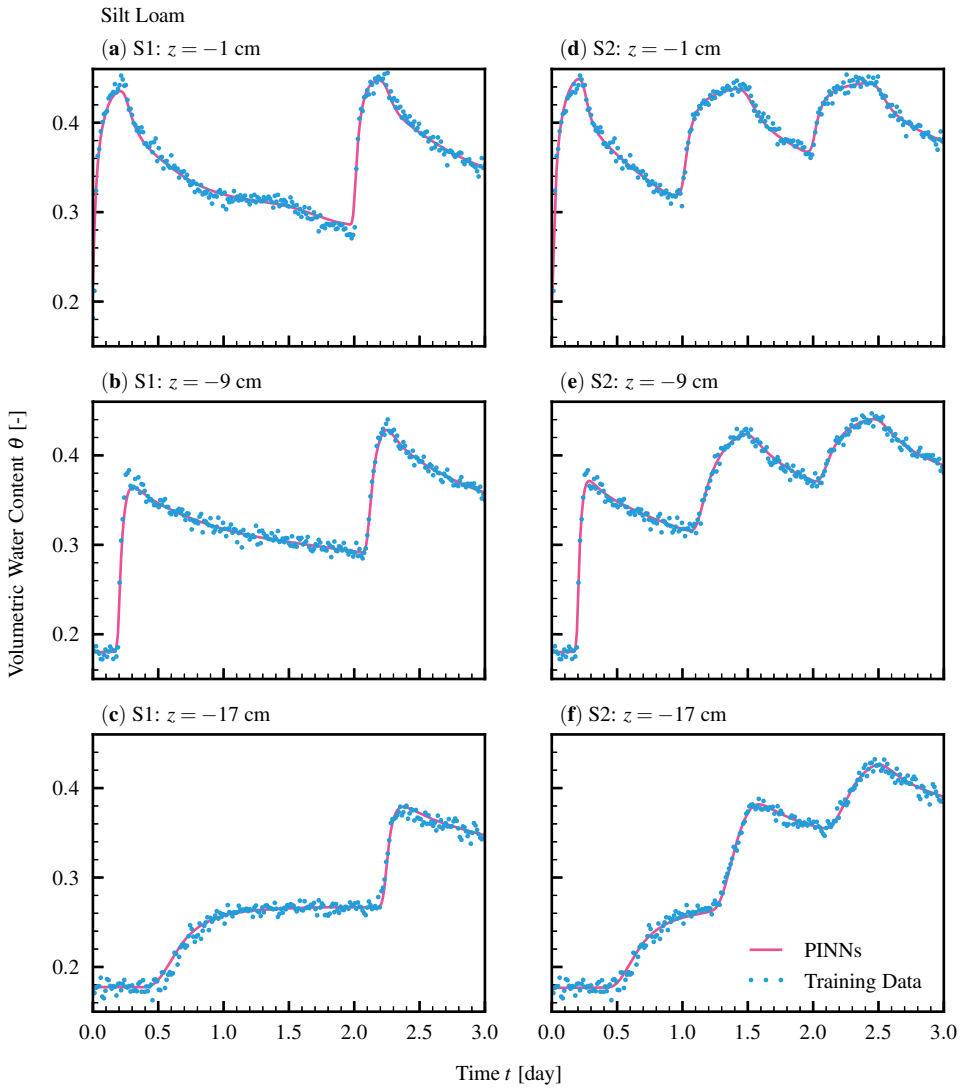

Figure S3. Predicted volumetric water content (PINNs) and noisy synthetic training data (Training Data) for silt loam soil for the two scenarios at three different depths. Scenario 1 (S1): (**a**) $z = -1$ cm, (**b**) $z = -9$ cm, and (**c**) $z = -17$ cm. Scenario 2 (S2): (**d**) $z = -1$ cm, (**e**) $z = -9$ cm, and (**f**) $z = -17$ cm.

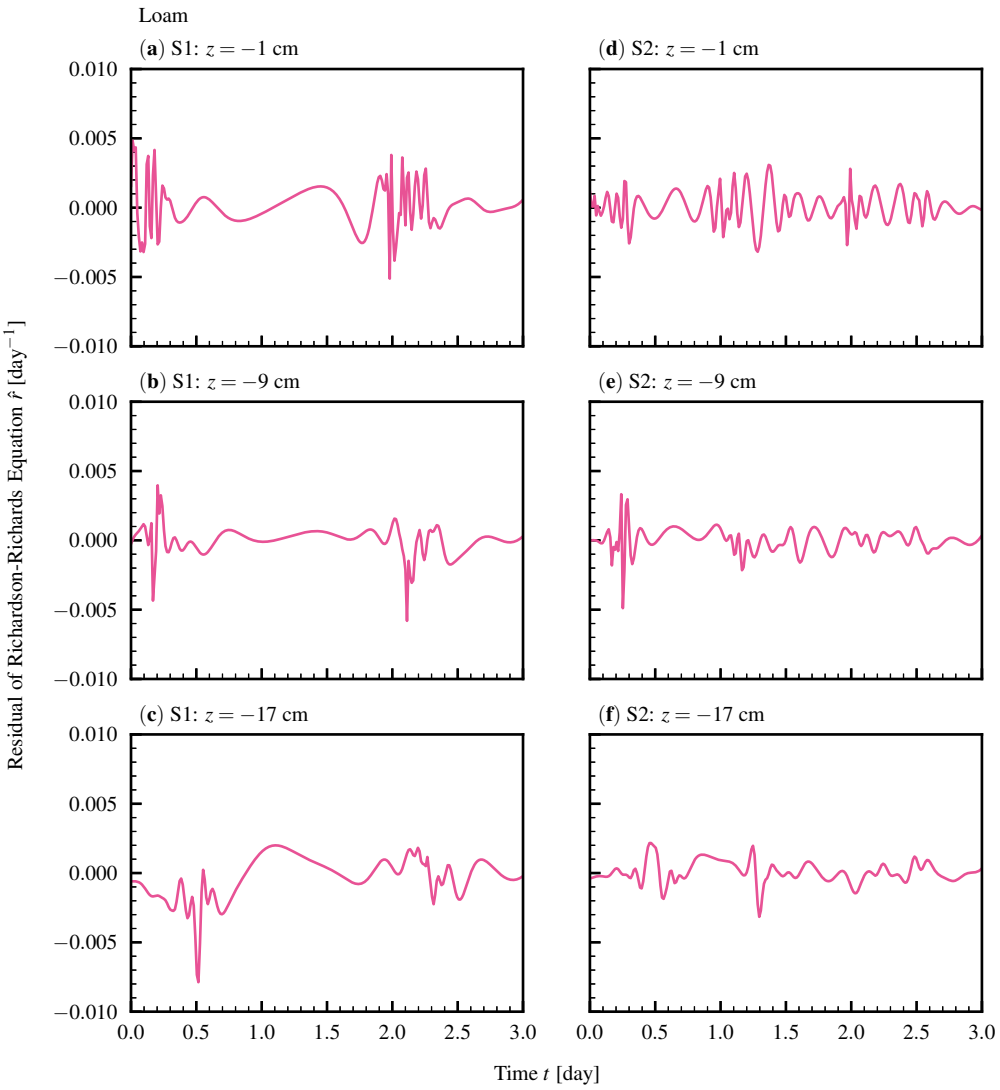

Figure S4. The residuals of the Richardson-Richards equation at three different depths for loam soil for the two scenarios. Scenario 1 (S1): (**a**) $z = -1$ cm, (**b**) $z = -9$ cm, and (**c**) $z = -17$ cm. Scenario 2 (S2): (**d**) $z = -1$ cm, (**e**) $z = -9$ cm, and (**f**) $z = -17$ cm.

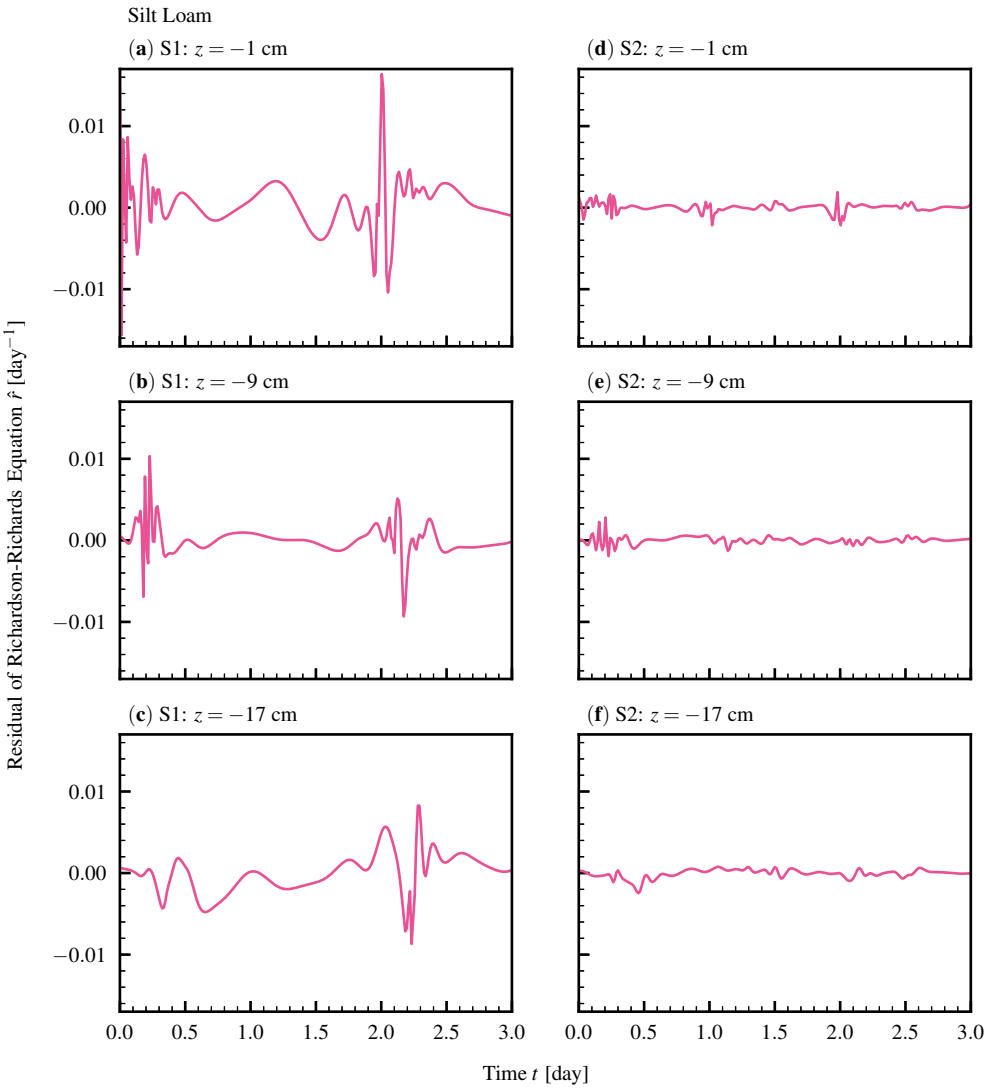

Figure S5. The residuals of the Richardson-Richards equation at three different depths for silt loam soil for the two scenarios. Scenario 1 (S1): (**a**) $z = -1$ cm, (**b**) $z = -9$ cm, and (**c**) $z = -17$ cm. Scenario 2 (S2): (**d**) $z = -1$ cm, (**e**) $z = -9$ cm, and (**f**) $z = -17$ cm.

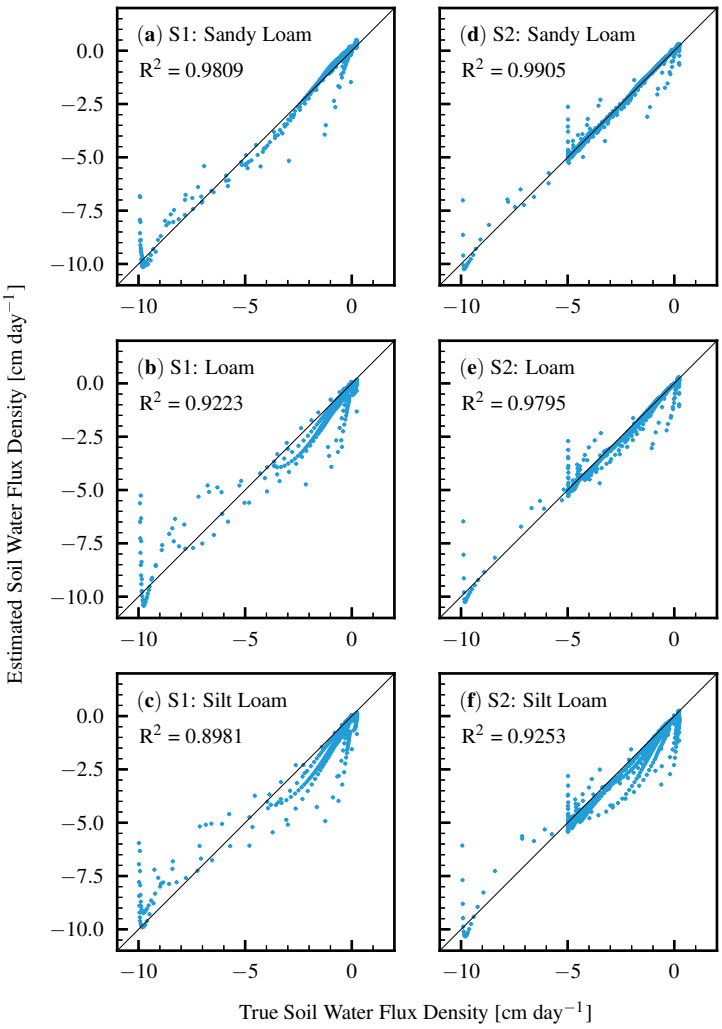

Figure S6. Comparison of the true soil water flux density to the one predicted by the PINNs for the three soils and the two scenarios. Scenario 1 (S1): (**a**) sandy loam, (**b**) loam, and (**c**) silt loam. Scenario 2 (S2): (**d**) sandy loam, (**e**) loam, and (**f**) silt loam.

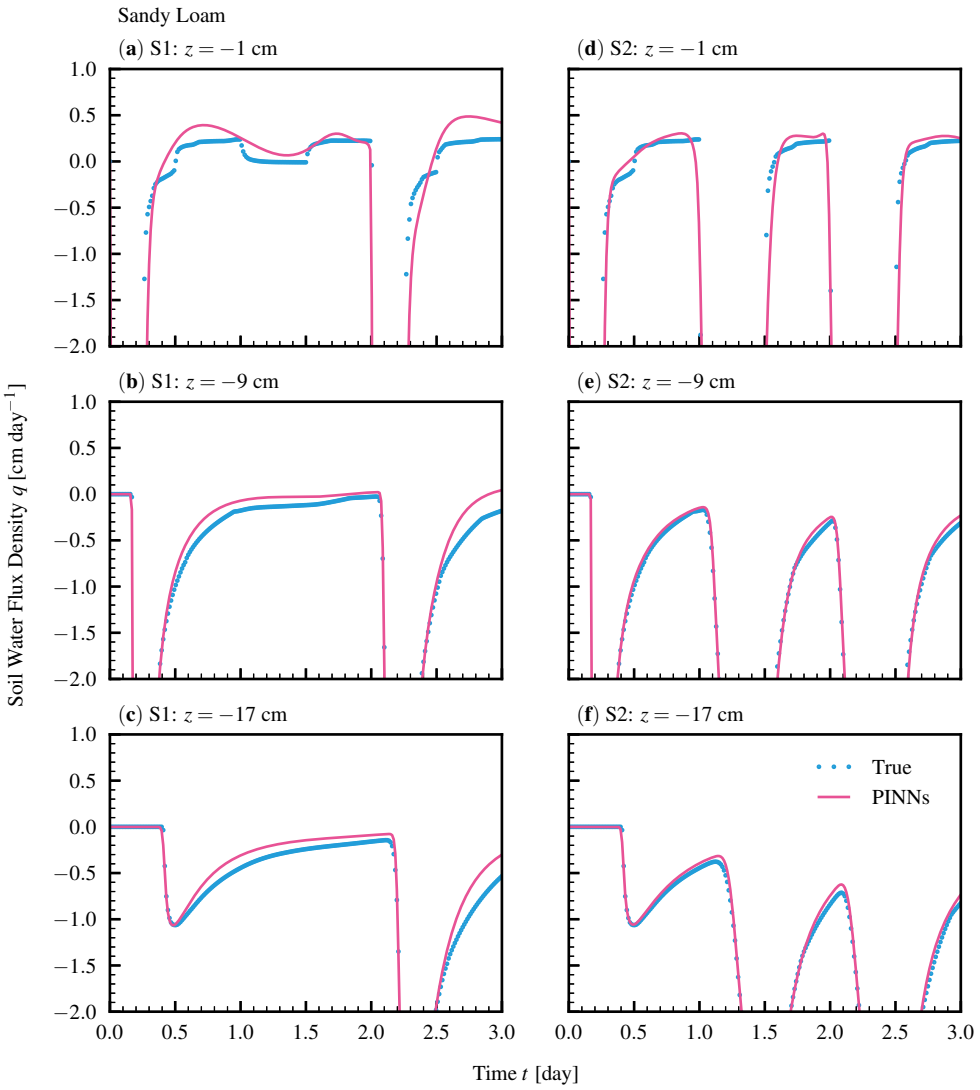

Figure S7. Estimated soil water flux density against the true one for a limited range at three different depths for sandy loam soil. Scenario 1 (S1): (**a**) $z = -1$ cm, (**b**) $z = -9$ cm, and (**c**) $z = -17$ cm. Scenario 2 (S2): (**d**) $z = -1$ cm, (**e**) $z = -9$ cm, and (**f**) $z = -17$ cm.

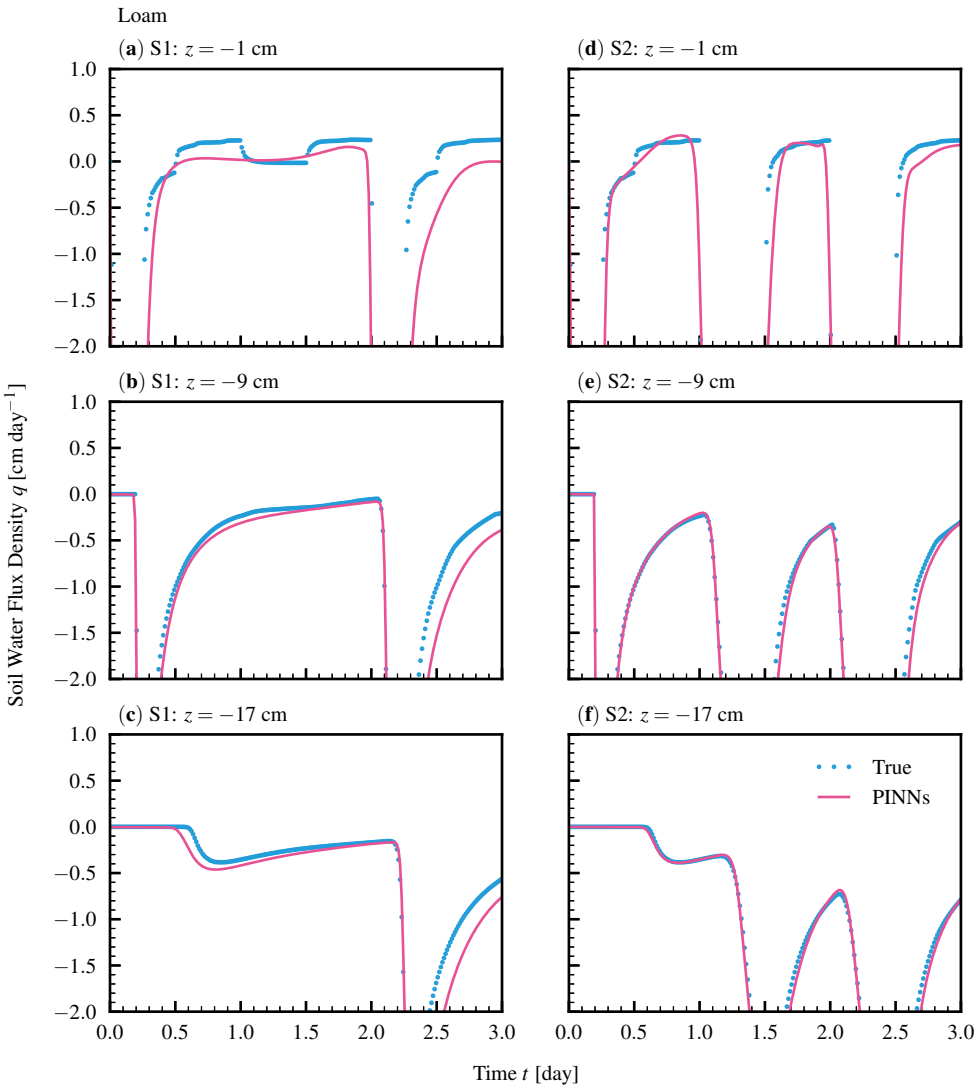

Figure S8. Estimated soil water flux density against the true one for a limited range at three different depths for loam soil. Scenario 1 (S1): (**a**) $z = -1$ cm, (**b**) $z = -9$ cm, and (**c**) $z = -17$ cm. Scenario 2 (S2): (**d**) $z = -1$ cm, (**e**) $z = -9$ cm, and (**f**) $z = -17$ cm.

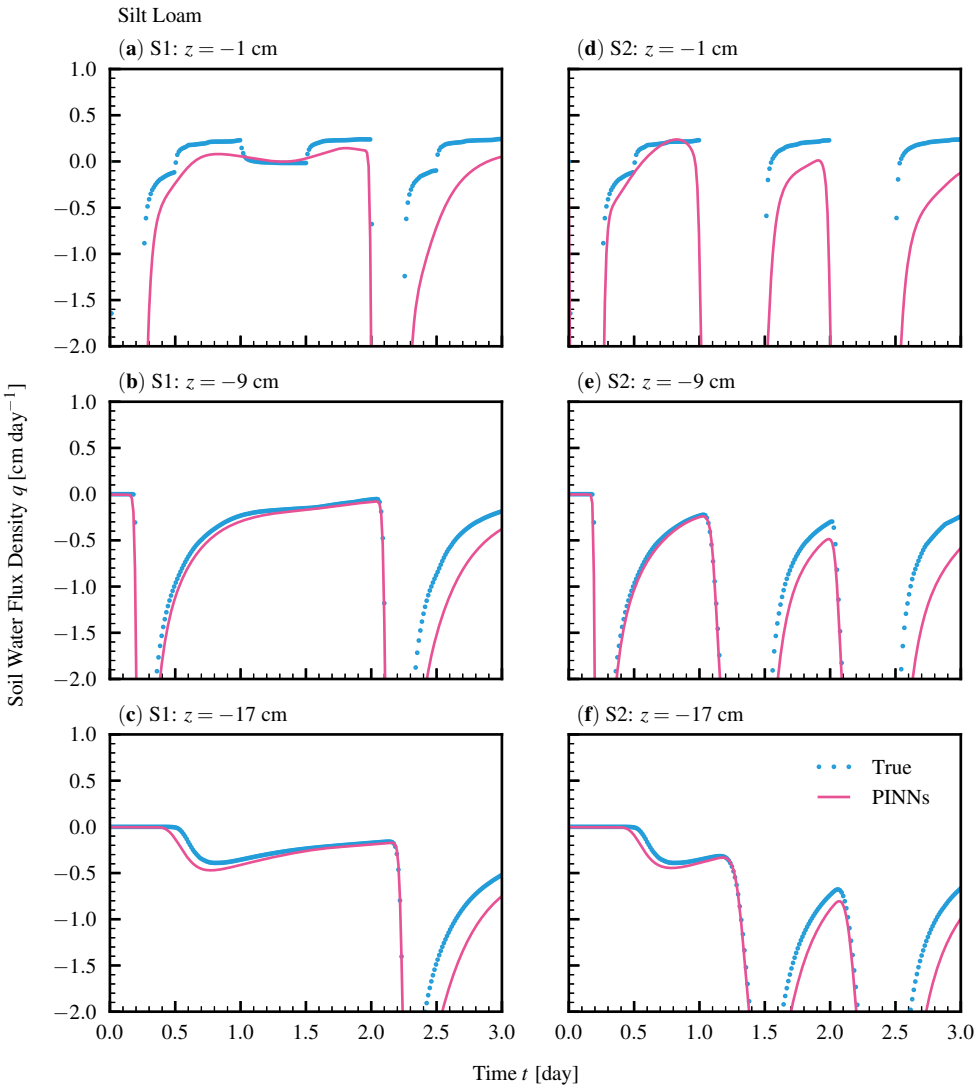

Figure S9. Estimated soil water flux density against the true one for a limited range at three different depths for silt loam soil. Scenario 1 (S1): (**a**) $z = -1$ cm, (**b**) $z = -9$ cm, and (**c**) $z = -17$ cm. Scenario 2 (S2): (**d**) $z = -1$ cm, (**e**) $z = -9$ cm, and (**f**) $z = -17$ cm.

Table S1. The coefficient of determination R^2 between predicted volumetric water content and the synthetic training data with different amount of noise for Scenario 1. The architecture of the PINNs is fixed.

Standard Deviation of Noise	Sandy Loam	Loam	Silt Loam
0	0.9987	0.9990	0.9994
0.005	0.9988	0.9949	0.9942
0.01	0.9985	0.9985	0.9959
0.02	0.9965	0.9976	0.9978

Table S2. The coefficient of determination R^2 between predicted volumetric water content and the synthetic training data without noise for Scenario 1 for sandy loam soil and for different numbers of hidden layers and units for each hidden layer of the neural network for predicted matric potential.

	Units		
Hidden Layers	10	20	40
2	0.9281	0.9746	0.9878
4	0.9787	0.9855	0.9964
6	0.9762	0.9966	0.9987
8	0.9821	0.9974	0.9971
9	0.9957	0.9989	0.9987
10	0.9965	0.9982	0.9987
11	0.9968	0.9984	0.9990

Table S3. The coefficient of determination R^2 between predicted volumetric water content and the synthetic training data without noise for Scenario 1 for loam soil and for different numbers of hidden layers and units for each hidden layer of the neural network for predicted matric potential.

	Units		
Hidden Layers	10	20	40
2	0.8201	0.9757	0.9870
4	0.9472	0.9958	0.9977
6	0.9595	0.9973	0.9983
8	0.9946	0.9982	0.9985
9	0.9975	0.9979	0.9944
10	0.9958	0.9864	0.9990
11	0.9973	0.9990	-0.3224

Table S4. The coefficient of determination R^2 between predicted volumetric water content and the synthetic training data without noise for Scenario 1 for sandy loam soil for different numbers of units in the hidden layer of the neural networks for predicted volumetric water content $\hat{\theta}$ and hydraulic conductivity $\hat{K}$. The architecture of the neural network for the predicted matric potential is fixed.

	Units for $\hat{K}$		
Units for $\hat{\theta}$	5	10	20
5	0.9990	0.9987	0.9993
10	0.9956	0.9984	0.9974
20	0.9996	0.9993	0.9987

Table S5. The coefficient of determination R^2 between predicted volumetric water content and the synthetic training data without noise for Scenario 1 for loam soil for different numbers of units in the hidden layer of the neural networks for predicted volumetric water content $\hat{\theta}$ and hydraulic conductivity $\hat{K}$. The architecture of the neural network for the predicted matric potential is fixed.

	Units for $\hat{K}$		
Units for $\hat{\theta}$	5	10	20
5	0.9946	0.9942	0.9960
10	0.9993	0.9981	0.9982
20	-0.3222	0.9929	0.9990

Table S6. The coefficient of determination R^2 between predicted volumetric water content and the synthetic training data without noise for Scenario 1 for silt loam soil for different numbers of units in the hidden layer of the neural networks for predicted volumetric water content $\hat{\theta}$ and hydraulic conductivity $\hat{K}$. The architecture of the neural network for the predicted matric potential is fixed.

	Units for $\hat{K}$		
Units for $\hat{\theta}$	5	10	20
5	0.9988	0.9988	0.9991
10	0.9994	0.9983	0.9988
20	0.9993	0.9996	0.9994